CHAPTER 5

SYNTHESIS OF PVDF/TiO_2 MEMBRANES AND THEIR ANTIFOULING BEHAVIOUR DURING ULTRAFILTRATION

In this chapter the synthesized PVDF/TiO_2 nanocomposite via phase inversion route were characterized by permeation tests using Bovine Serum Albumin (BSA) as a model foulant. The BSA filtration experiments have revealed that membrane with 2 wt% of TiO_2 (PM3) exhibits excellent permeation flux, high rejection ratio, and shows good antifouling performance. The adsorption capacity of bovine serum albumin on the membrane surface decreased from 2.85 to 2.15 mg cm^{-2} as the TiO_2 loading increased from 0 to 3 wt% with respect to polymer. Fouling has been found due to cake formation in Ultrafiltration and can be explained by the Hermia's fouling model suggesting that the solutes are not deposited into the pores which interpret that the fouling process is physically reversible.

5.1 INTRODUCTION

Due to non-toxic nature, reasonably high chemical resistance, and relatively low cost, polyvinylidene fluoride (PVDF) is one of the widely used polymers for making membranes for ultrafiltration (UF). However, high hydrophobicity restricts its application and fouling reduces its performance. Fouling of MF and UF membranes due to proteins has been ascribed to adsorption and deposition of proteins on the surface of membranes and within their pores (Marshall et al., 1993). Membrane fouling of UF membranes strongly affects the economic and technological viability of the separation process (Salahi et al., 2010). The fouling is normally classified as reversible fouling which can be easily reversed by physical methods and irreversible fouling which requires special pre-treatment techniques for its elimination (Bhattacharya et al., 2001).Reversible fouling can be eliminated by physical

cleaning because the solutes are externally deposited on the membrane, whereas irreversible fouling requires chemical cleaning (Etemadi et al., 2018) because solutes are accumulated inside the pores and the binding force of particles is higher compared to reversible fouling. The chemical cleaning affects the membrane material thus in turn adversely affecting membrane life. This has necessitated the modification of membranes to improve the performance by eliminating fouling.

Various techniques used for improving the performance of PVDF membranes include physical blending with hydrophilic fillers (polymers or inorganic), grafting of hydrophilic species, and plasma treatment to improve the hydrophilicity (Behboudi et al., 2016). The weak interaction during physical blending of the polymer and additives reduce the long-term durability and cause instability due to an additive release from the membranes (Zhao et al., 2014). Recently, nanocomposite membranes, i.e. polymeric membranes embedded with uniformly dispersed inorganic nanoparticles (NPs) have attracted the attention of researchers due to the unique physicochemical properties of NPs (Akbari et al., 2016). Incorporation of NPs in the polymer matrix alters the porous structure and improves hydrophilicity, mechanical and thermal resistance, permeability and antifouling properties (Zhao et al., 2014). Nano-particles of TiO_2 (Jafarzadeh and Yegani 2015), ZnO (Balta et al., 2012), and SiO_2 (Zuo et al., 2014), GO (Zhao et al., 2014) have been widely used for the synthesis of polymer-inorganic composite membranes (Zinadini et al., 2015).

A better understanding of fouling of the membrane is important to solve the problems encountered during its application. A knowledge of the membrane fouling is advantageous for determining the capacity and efficiency of the membranes. Several empirical and mathematical models have been developed to explain the fouling mechanism (Vela et al., 2008). The mathematical models are useful for optimization of fouling removal and

prevention methods along with a better understanding of the filtration phenomena for different membranes in the real-world scenario. Completely theoretical models have failed to explain the permeate flux decline during ultrafiltration without using experimental data (Charfi et al., 2012). Therefore semi-empirical models that permit accurate prediction of the flux decline during ultrafiltration and offer explanation to the process of fouling are preferred. Hermia's model is one of such models that has been used in this work to quantify the properties of the membrane by fitting the experimental results for explaining the fouling mechanism in order to adapt the process for controlling the fouling. The parameters of this model, have a physical meaning and it is based on the classical constant pressure filtration equations and unlike other models it does not involve complex mathematical equations.

The PVDF membranes incorporated with different amounts of green synthesized TiO_2 NPs were prepared via the phase inversion method. The antifouling performance of the synthesized membranes (both pure PVDF and PVDF/TiO_2 nano-composite) was investigated using bovine serum albumin (BSA) as the model foulant. The Hermia model was used to investigate the fouling phenomenon and associated mechanism during UF process and also to quantify the membrane properties affecting fouling. The model predictions are compared with the experimental data. The details of these experiments and analysis of resultant data are presented in this chapter.

5.2 EXPERIMENTAL PROCEDURE

5.2.1 Materials

Polyvinylidenefluoride (PVDF), n-methyl-2-pyrrolidone (NMP), titanium isopropoxide (TTIP) were obtained from Sigma-Aldrich (Mumbai, India). Bovine serum albumin (BSA) was obtained from SD Fine Chemicals Ltd. (Mumbai, India), and

phosphate buffer saline (PBS) were obtained from Merck, (Mumbai, India), Double distilled water (DD) used in all experimentswas prepared in the laboratory.

5.2.2 Synthesis of TiO_2 nanoparticles (NPs) and PVDF/TiO_2 composite membrane preparation

The particle and membrane were synthesized as already described in Sections 3.2.2 (a) and 3.2.2(b) of Chapter 3.

5.2.3 BSA Adsorption Experiment

The pure PVDF and nano-composite membranes of size 1 × 1 cm^2 were taken and immersed into 5 mL of BSA solution (0.5 g/L in 5 mM PBS, pH=7.5) till equilibrium was established (for 24 hours) to study extent of adsorption at room temperature. The membrane samples with adsorbed BSA were removed, and the remaining solution in the vials was agitated in a shaker. The BSA concentration was measured using a UV spectrophotometer (SYSTRONICS, PC Based Double Beam Spectrometer 2202, India). To minimize error, each reported value was obtained by averaging five individual measurements. The BSA adsorption capacity was determined using equation 5.1 (Teow et al., 2017)

$$\text{Adsorption capacity} = \frac{C_o - C}{A} \times V \qquad (5.1)$$

where A is the area of membrane (m^2), V is the total volume (0.005 L), and C_o and C are the concentration (g/L) of BSA before and after contact with the membranes.

5.2.4. Quantification of fouling

The effect of TiO_2 loading on membrane performance and fouling behavior was investigated using BSA as the model foulant. The BSA solution was prepared by dissolving

1 g BSA in 1 L of 1mM of PBS solution at pH 7.5. The filtration experiments were carried out in a dead-end filtration setup as shown in Figure 5.1.

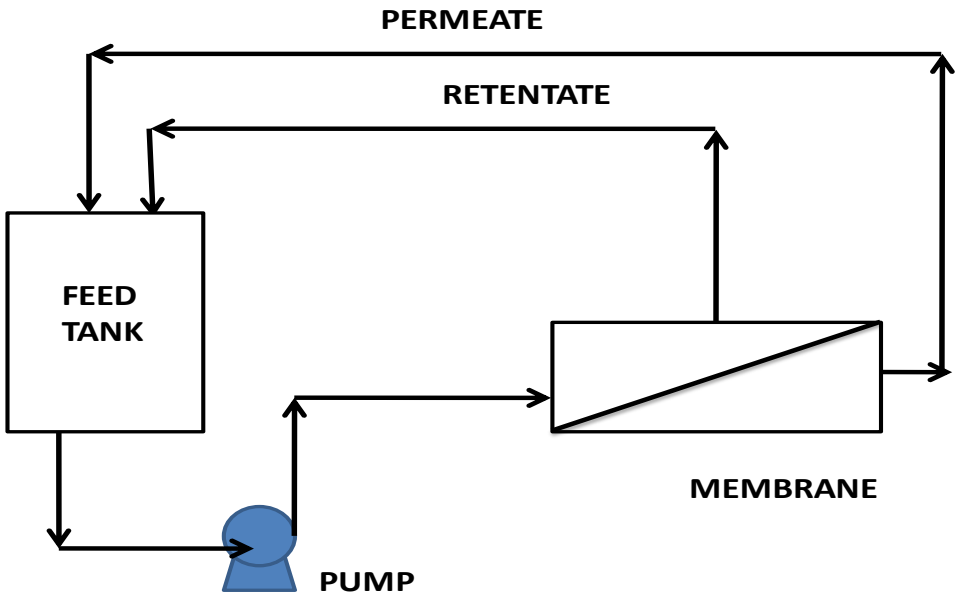

Figure 5.1: The dead-end filtration cell

The effective membrane area for filtration was 15.5 $cm^{2.}$ The membranes were initially pre-pressurized for 30 min at 2 bar to achieve stable water flux. After pure water flux measurement (J_{w1}) tests, the flux for BSA solution was measured (J_{BSA}) and recorded every 10 min to determine the dynamic fouling resistance. After 2 h of BSA filtration, the used membrane was taken out of the cell, rinsed with distilled water for 30 min with magnetic stirring and then, second pure water flux (J_{w2}) was again measured. All the measurements were carried out at 2 bar and 27±°C. Concentrations of BSA in feed(C_f) and permeate(C_p) were determined using UV spectrophotometer and the flux recovery ratio was calculated using Equation 5.2.

Flux recovery ratio (FRR) = $\frac{J_{w2}}{J_{w1}}$ x 100 (5.2)

5.2.5 Fouling Resistance

The loss in flux can be quantified in terms of total fouling ratio (TFR), reversible fouling ratio (RFR),and irreversible fouling ratio (IFR) defined in terms of following equations 5.3, 5.4 and 5.5 (Etemadi et al., 2018)

$$\text{RFR \%} = \left(\frac{J_{w2} - J_{BSA}}{J_{w1}}\right) \times 100 \quad (5.3)$$

$$\text{IFR \%} = \left(\frac{J_{w1} - J_{w2}}{J_{w1}}\right) \times 100 \quad (5.4)$$

and

$$\text{TFR \%} = \text{RFR \%} + \text{IFR \%} = \left(\frac{J_{w1} - J_{BSA}}{J_{w1}}\right) \times 100 \quad (5.5)$$

The reversible fouling refers to the weak binding of foulant species to the membrane surface and can be eliminated easily by water washing. This is an important parameter as fouling of membrane increases the operational costs (Tian et al., 2013). The irreversible fouling, the foulants are strongly attached to the membrane surface and are removed by the chemical cleaning process. So, this type of fouling deteriorates the membrane lifetime along with increases the process complexity (Peldszus et al., 2011).

5.2.6 Hermia's Model of Fouling

Hermia's model, the most comprehensive fouling model, is used to identify the dominant mechanism responsible for membrane fouling under constant pressure filtration. The model provides a correlation between flux and operating time by assuming pore blockage, gel-polarization, and bio-fouling. In general mathematical form it is expressed as (Charfi et al., 2012):

$$\frac{d^2t}{dV^2} = \alpha\left(\frac{dt}{dV}\right)^n \quad (5.6)$$

here V is the cumulative volume of filtrate (m^3), α is the proportionality constant, t is the time of filtration, A is flow area (m^2), and n is the constant characterizing the fouling model. The flux (J) of the permeate is written as

$$J=\frac{1}{A}\frac{dV}{dt} \quad (5.7)$$

Equation 5.7 can be rewritten as

dt/dV=1/AJ

The second derivative of Equation 5.7 gives

$$\frac{d^2t}{dV^2}= = -\alpha A^{-2} J^{-3}\frac{dJ}{dt} \quad (5.8)$$

Equation 5.8 is proportional to the rate of increase in total resistance (Teow et al., 2017).The governing equation for flux decline with time now becomes

$$\frac{dJ}{dt} = -\alpha A^{2-n} J^{3-n} = -K_{CF} J^{3-n} \quad (5.9)$$

here K_{CF} is a phenomenological coefficient. This equation permits a deeper analysis of the fouling mechanisms taking place inside pores or onto the membrane surface. The model represented in Equation 5.9 is used to distinguish four possible fouling mechanisms and their phenomenological coefficients.

Complete pore blockage **(n=2)**

The linear form of this model was derived by integrating Equation 5.9 with time and substituting n=2 as:

$$\ln\left(\frac{1}{J}\right)= \ln\left(\frac{1}{J_o}\right) + K_1 t \quad (5.10)$$

where J_o is initial permeate flux, J is flux at time t, K_1 is complete pore blocking coefficient, determined by evaluating the slope of the straight line fitting of Equation 5.10.

According to this model, the flux decline is due to the deposition of the solute aggregates of larger size compared to membrane pore opening on the membrane surface thereby decreasing the available pores for the filtrate to pass through it or in other words sealing the entrance of the pores.

Standard pore blocking **(n=1.5)**

This approach accounts for the fouling occurring within the internal structure of the membrane. The reduction of pore radii is due to deposition or adsorption of the solute onto the internal pore walls. Taking the value of exponent n in Equation 5.9 as 1.5 and integrating it to give the linear form of flux decline relation with time gives:

$$\left(\frac{1}{\sqrt{J}}\right) = \left(\frac{1}{\sqrt{J_o}}\right) + K_2 t \qquad (5.11)$$

where K_2 represent internal pore blocking coefficient, it is determined by evaluating the slope from the straight line fitting of Equation 5.11.

Intermediate pore blockage **(n=1)**

This situation is similar to the complete pore blockage. Also, it assumes partial blockage or obstruction of the entrance of the pore without completely blocking it. Particles here get deposited on the pores wall thus reducing the pore volume. The irregularity of passage through pore causes the particle tightly attached to the pore. Substituting n= 1 in Equation 5.9 and integrating with time the linear form of flux decline as:

$$\left(\frac{1}{J}\right) = \left(\frac{1}{J_o}\right) + K_3 t \qquad (5.12)$$

where K_3 represents intermediate pore blocking coefficient,which is determined from the slope of the straight line plot of Equation 5.12.

***Cake Filtration* (n=0)**

In contrast to the above-described models, here it is assumed that the fouling occurs by the formation of cake over the membrane surface thereby increasing the hydraulic resistance. The overall resistance is a combination of cake resistance and resistance of membrane. The filtration model is obtained by substituting n= 0 and integrating equation 5.9

$$\left(\frac{1}{J^2}\right) = \left(\frac{1}{J_o^2}\right) + K_4 t \qquad (5.13)$$

Here K_4 represents cake pore block coefficient. It is determined from the slope of the straight line plot of equation 5.13.

5.3 RESULTS AND DISCUSSION

5.3.1 BSA Adsorption Test

The TiO_2 incorporated PVDF membranes exhibit enhanced hydrophilicity due to the presence of hydrophilic TiO_2 within the polymer matrix. The enhanced hydrophilicity directly improves the anti-fouling properties of membranes. In order to ascertain this static protein adsorption was investigated to study the anti-fouling properties.

Figure 5.2 shows that the amount of BSA adsorption decreases with increase in TiO_2 loading from 0 to 2 wt%. The decreased adsorption values suggest increased antifouling ability. It is attributed to the fact that the presence of abundant surface hydroxyl groups on the entrapped TiO_2 nano-particles weakens the hydrophobic interaction of membranes with BSA, and thus decreases the adsorption and its attachment to the surface. The increased adsorption in case of membranes having 3 wt% TiO_2 can be attributed to the aggregation of TiO_2 particles at higher concentrations leading to its uneven distribution

within the membrane matrix thus resulting in the availability of more sites for protein (or foulant) adsorption.

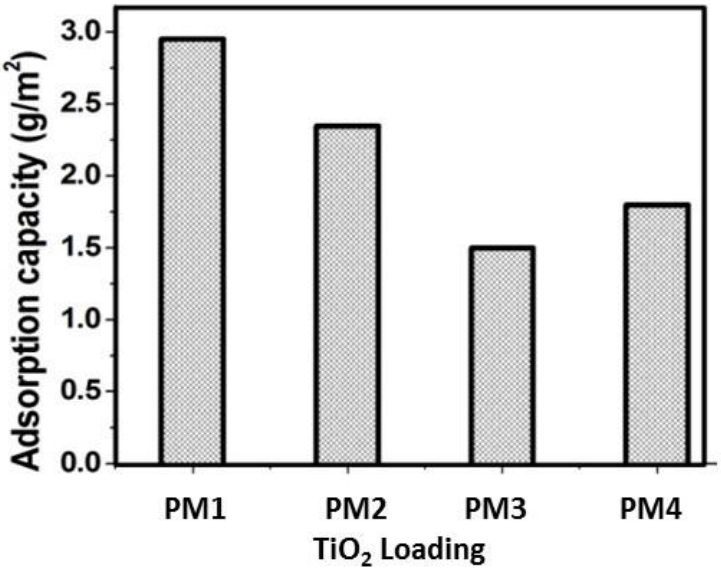

Figure 5.2: Adsorption capacity of composite membrane at different TiO_2 loading

5.3.2 Water Permeation

Figure 5.3 shows the effect of TiO_2 loading in the membrane on the pure water flux before and after BSA filtration. It is seen that the increase in the water flux was observed in TiO_2 incorporated membranes and the water flux increment follows the same trend as hydrophilicity with respect to particle loading as described in section 3.2.2.b of chapter 3. It can be concluded that the increased membrane hydrophilicity, increases the water permeability by attracting water molecules and facilitating permeation through the membrane. Moreover, the enhancement in the flux is due to increase in porosity and pore size. During the phase inversion process, increase in the diffusion of solvent from the membrane to water facilitates the formation of large number of micro-pores, leading to the formation of a porous membrane (Zinadini et al., 2014). It is seen that the TiO_2 incorporated membrane with the highest loading (PM4), gives lesser water flux than PM2

and PM3 membranes. This is attributed to the aggregation of nano-particles at high concentrations (Tian et al., 2013) reduces membrane pores and also the particle aggregation causes uneven distribution of particles within the membrane results in the availability of more sites for protein (or foulant) adsorption, resulting in a decline in the pure water flux. In this study, the maximum pure water flux was achieved for membrane PM3 with optimumTiO_2 loading of 2 wt%. This can be attributed to the proper dispersion of inorganic nano-particles and this can be taken as the optimum loading.

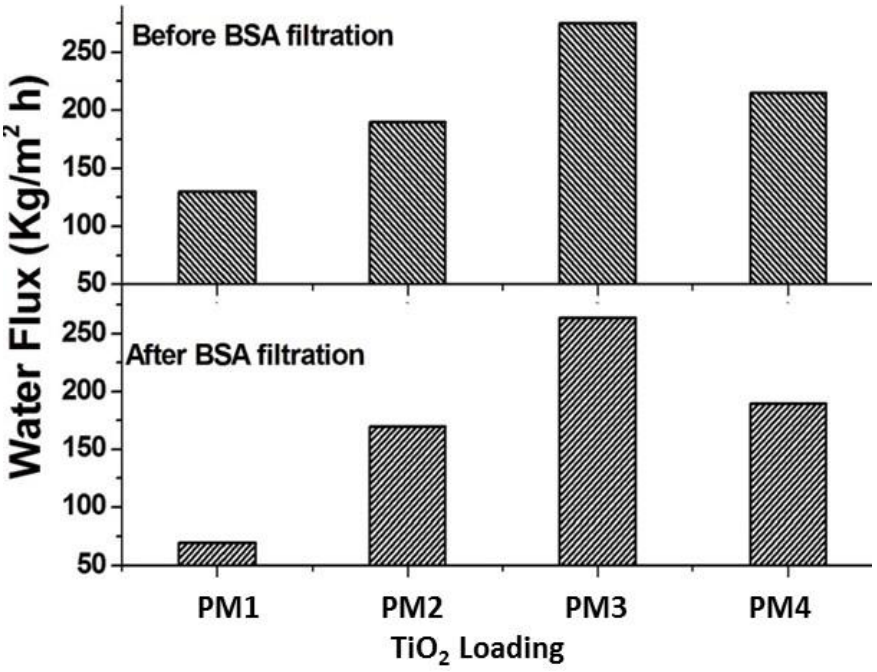

Figure 5.3: Pure water flux before and after BSA filtration

To further investigate the antifouling property of TiO_2 incorporated PVDF membranes, the flux recovery ratio (FRR (%)) and fouling resistance were also evaluated and are shown in Figure 5.4 a & b. A high value of FRR indicates better antifouling property of the membrane. The FRR in case of PVDF membrane was only 53.85% which was very small compared to hybrid membranes (FRR >85%). The maximum FRR value (96%) was obtained for PM3 membrane. The results of FRR are in good agreement with

the results of AFM studies shown in Table 4.1. The results show that the surface roughness of pure PVDF membranes is significantly higher than that of the hybrid membranes. The increase in rough surface increases the fouling of membrane due to protein accumulation within the ‘‘valleys’’ The membrane PM3 (2 wt% TiO_2) showed the lowest roughness, low contact angle, and high hydrophilicity, thus resulting in the best flux recovery ratio due to less deposition of foulant on the smoother surface (Figure 5.4a)

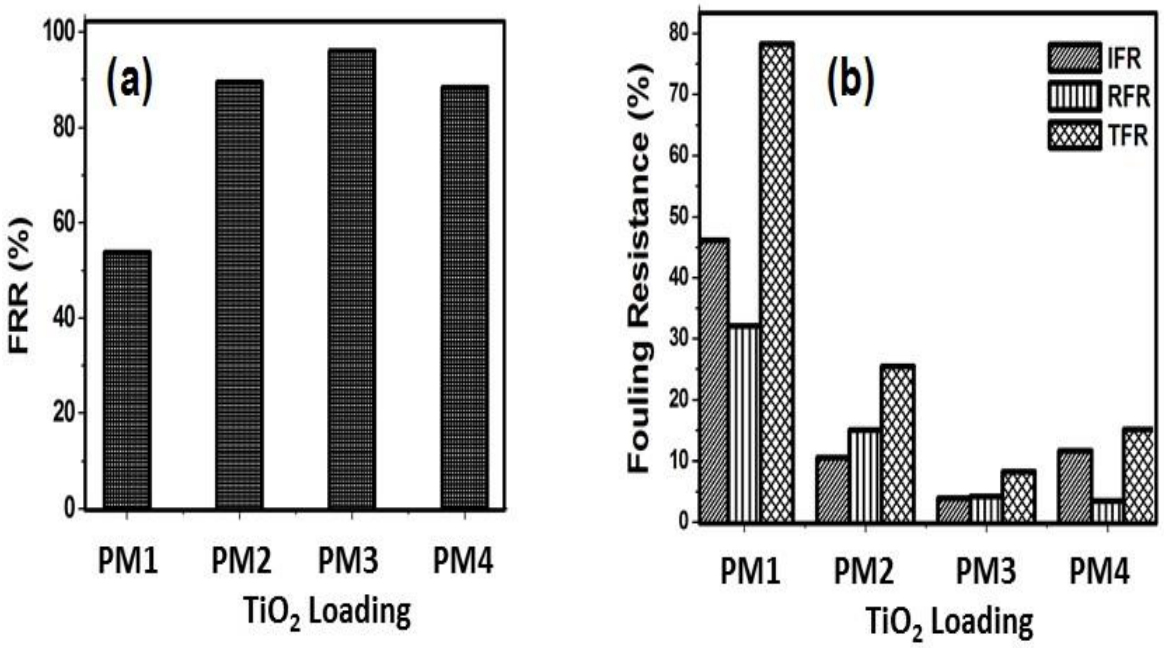

Figure 5.4: (a) FRR of membranes (b) Fouling resistance of membranes

The calculated TFR, RFR, and IFR values for various membranes are shown in Figure 5.4b.The figure shows that the pure membrane has the highest TFR (78.28%) and IFR (46.15%) values that are reduced significantly in case of composite membranes. This is attributed to the change in hydrophilic nature of surface due to the incorporation of TiO_2 NPs in the membrane matrix. Presence of NPs reduces the adsorption ability due to reduced interaction between the foulant and hydrophobic membrane interfaces (PM2, PM3, and PM4) this in turn promotes easy cleaning of BSA (foulant) by water flushing during

filtration. Further, the protective hydration layer over the membrane surface because of adsorption of water molecules due to the presence of hydrophilic TiO_2 NPs will exclude the BSA molecule more effectively (Peldszus et al., 2011). It was also observed that with increasing TiO_2 loading (PM2 and PM3) the resistance decreased.

5.3.3 Comparison of Experimental Results with Predictions using Hermia's Model

The Hermia's model has been used to study the decline in flux and various parameters calculated using the model are shown in Figure 5.5 and Table 5.1, respectively. The type of pore blocking model for fouling was selected based on the highest value of R^2 linear regression coefficient obtained using Equations (5.10) to (5.13).

If the size of foulant is smaller than the membrane pores, standard pore blocking occurs. From Figure 5.5 it is observed that the predictions from the standard pore blocking model deviate to a larger extent for all membranes from the experimental data, so it is not well accepted model for predicting fouling in the membrane. This is because most of the foulant will not be retained by the membrane at the operating conditions because most of the foulant present in feed solution is smaller than the membrane pores (Salahi et al., 2012). The predictions using complete pore blocking model are also similar. Large deviations observed between the model predictions and experimental values are due to large size of BSA (foulant) molecules.

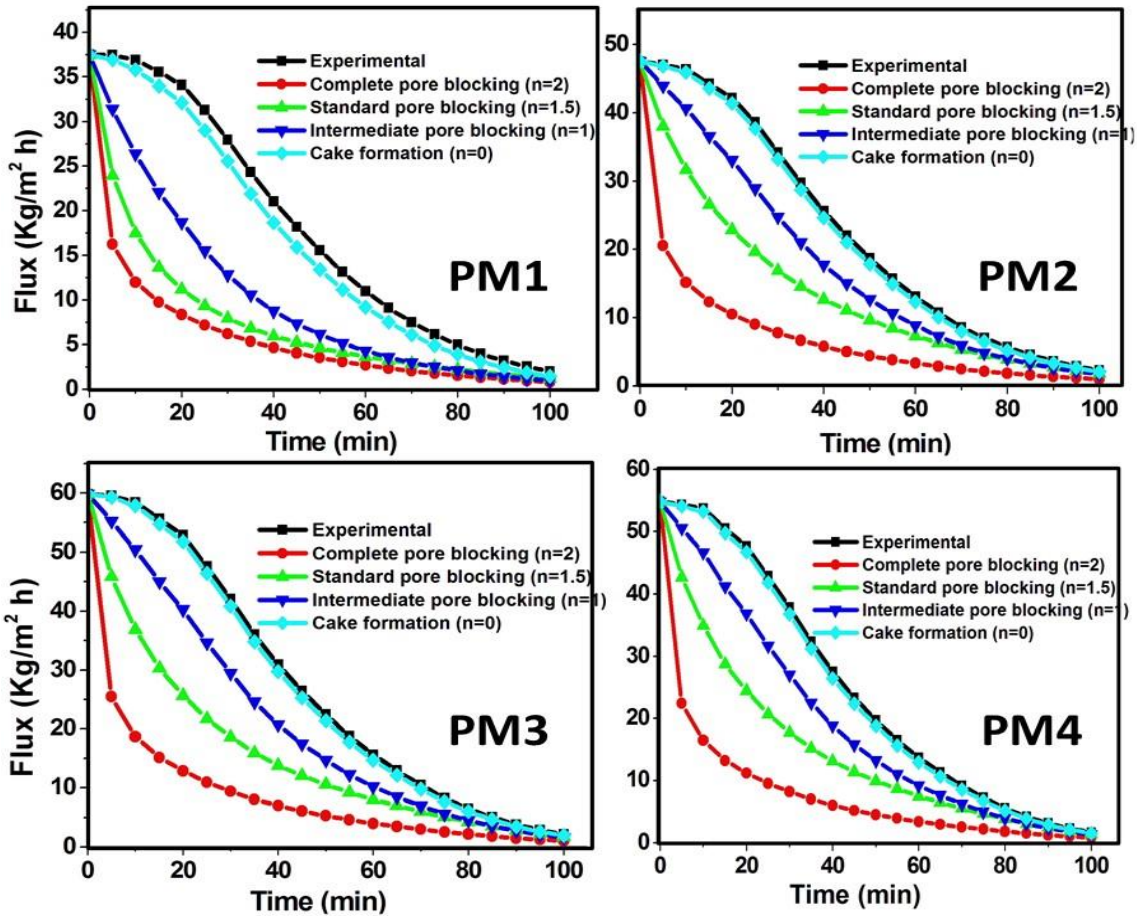

Figure 5.5: Comparison of experimental and predicted filtration data and classic fouling models for membrane

In case of intermediate pore blockage, when the size of membrane pores is similar to the foulant molecular size, the entrance of the pores on the feed side is blocked. However, the predicted flux, in this case, shows a better agreement with the experimental data compared to the standard and complete pore blockage models. Further, it has been reported that the UF is accurately described by the intermediate pore blocking model (Salahi et al., 2010). The pore blockage due to cake formation occurs when the solute size is larger than the membrane pore size as a result the solute molecules are not able to enter the membrane pores and accumulate over the surface forming a layer. The deposition of the solute layer over the membrane surface exerts additional resistance to the fluid flow

through the membrane (Fonouni et al., 2017). In this case the predicted values are in very good agreement with the experimental flux data (Figure5.5) under the experimental conditions. The high R^2 value indicates a better fit for this model.

Thus it can be inferred that the fouling mechanisms are the cake formation and intermediate pore blockage. Thus it can be concluded that most of the area of the fouled membrane gets covered due to cake formation while over some area the foulant particles enter the pores and lead to pore-constrictions. Table 5.1 shows that the pore blockage coefficients in all cases decline with increasing concentration of TiO_2 and is having the least value for cake filtration (n=0). This implies that as the rate of deposition of foulant over the membrane reduces the concentration polarization gets alleviated leading to a reduction in the cake layer fouling (Fonouni et al., 2017).

Table 5.1: Values of Ks and R^2 for composite membranes predicted using Hermia's fouling models

Sample	Cake pore		Intermediate pore		Standard pore		Complete	
	n=0		n=1		n=1.5		n=2	
	R^2	K_4	R^2	K_3	R^2	K_2	R^2	K_1
PM1	0.897	0.030	0.77	0.150	0.621	0.210	0.394	0.230
PM2	0.944	0.003	0.88	0.129	0.811	0.110	0.648	0.180
PM3	0.959	0.002	0.91	0.099	0.840	0.101	0.683	0.150
PM4	0.957	0.001	0.92	0.011	0.860	0.014	0.683	0.018

From the foregoing discussion it can be inferred that under the conditions investigated, gel layer formation is the main cause of membrane fouling. Such type of fouling is physically reversible.

5.4 CONCLUSION

Low fouling membranes using PVDF as a polymer base and TiO_2 nano-particles as an additive (synthesized by a green route) were prepared using the phase inversion technique. The TiO_2 dispersion within PVDF membrane plays a significant role in the membrane antifouling property. The ultra-filtration performance and anti-fouling property of the membrane were investigated using BSA as the model foulant. The low values of TFR and IFR for nano-composite membrane suggested that addition of very small quantity of TiO_2 nanoparticles (2 wt%) enhanced the resistive fouling property of membrane by decreasing the irreversible fouling followed by an increase in the portion of reversible fouling. This will result in easy removal of fouling by physical cleaning. The fouling was also analyzed using four modes of Hermia's fouling model and it was observed that the "cake filtration" model gave the best prediction which further justifies that fouling process is physically reversible

5.5 REFERENCE

Akbari A, Yegani R, Pourabbas B, Behboudi A, Fabrication and study of fouling characteristics of HDPE/PEG grafted silica nanoparticles composite membrane for filtration of humic acid. Chemical Engineering Research and Design 109(2016) 282–296.

Balta S, Sotto A, Luis P, Benea L, Van der Bruggen B, Kim J, A new outlook on membrane enhancement with nanoparticles: the alternative of ZnO, Journal of Membrane Science 389 (2012) 155–161.

Behboudi A, Jafarzadeh Y, Yegani R, Preparation and characterization of TiO2 embedded PVC ultrafiltration membranes, Chemical Engineering Research and Design 114 (2016) 96–107.

Bhattacharya PK, Agarwal S, De S, Rama Gopal UVS, Ultrafiltration of sugar cane juice for recovery of sugar: analysis of flux and retention. Separation and Purification Technology 21 (2001) 247–259.

Charfi A, Ben Amar N, Harmand J, Analysis of fouling mechanisms in anaerobic membrane bioreactors. Water Research 46(2012)2637–2650.

Etemadi H, Yegani R, Seyfollahi M, Rabiee M, Synthesis, characterization, and anti-fouling properties of cellulose acetate/polyethylene glycol-grafted nanodiamond nanocomposite membranes for humic acid removal from contaminated water. Iranian Polymer Journal (2018) 27:381–393.

Fonouni M, Etemadi H, Yegani R, Zarin S, Fouling characterization of TiO_2 nanoparticle embedded polypropylene membrane in oil refinery wastewater treatment using membrane bioreactor (MBR). Desalination and Water Treatment 90 (2017)99.

Jafarzadeh Y, Yegani R, Analysis of fouling mechanisms in TiO_2 embedded high density polyethylene membranes for collagen separation. Chemical Engineering Research and Design 93 (2015) 684–695.

Marshall AD, Munro PA, Tragardh G, The effect of protein fouling in microfiltration and ultrafiltratin on permeate flux, protein retention and selectivity - a literature-review. Desalination 91 (1) (1993) 65–108.

Peldszus S, Hallé C, Peiris RH, Hamouda M, Jin X, Legge RL, Budman H, Moresoli C, Huck PM, Reversible and irreversible low-pressure membrane foulants in drinking water treatment: identification by principal component analysis of fluorescence EEM and mitigation by biofiltration pretreatment. Water Research 45 (2011) 5161–5170

Salahi A, Abbasi M, Mohammadi T, Permeate flux decline during UF of oily wastewater: Experimental and modelling. Desalination 251 (2010) 153–160.

Teow YH, Ooi BS, Ahmad AL, Fouling behaviours of PVDF-TiO_2 mixed-matrix membrane applied to humic acid treatment. Journal of Water Process Engineering 15 (2017) 89–98.

Tian J-Y, Ernst M, Cui F, Jekel M, Correlations of relevant membrane foulants with UF membrane fouling in different waters. Water Research 47 (2013) 1218– 1228.

Vela M C V, Blanco S, Garcı´a JL, Rodrı´guez E B Analysis of membrane pore blocking models applied to the ultrafiltration of PEG. Separation and Purification Technology 62 (2008) 489–498.

Zhao C, Xu X, Chen J, Wang G, Yang F, Highly effective antifouling performance of PVDF/graphene oxide composite membrane in membrane bioreactor (MBR) system. Desalination 340 (2014) 59–66.

Zinadini S, Vatanpour V, Zinatizadeh AA, Rahimi M, Rahimi Z, Kian M, Preparation and characterization of antifouling grapheme oxide/polyethersulfone ultrafiltration membrane: application in MBR for dairy wastewater treatment. Journal of Water Process Engineering 7 (2015) 280–294.

Zinadini S, Zinatizadeh AA, Rahimi, M, Vatanpour V, Zangeneh H, Preparation of a novel antifouling mixed matrix PES membrane by embedding graphene oxide nanoplates. Journal of Membrane Science 453 (2014) 292–301.

Zuo X, Wang L, He J, Li Z, Yu S, SEM-EDX studies of SiO_2/PVDF membranes fouling in electrodialysisof polymer-flooding produced wastewater: diatomite, APAM and crude oil. Desalination 347 (2014) 43–51.